Chapter VII

Reversible Protonated Resting State of the Nitrogenase Active Site

Reproduced with permission from *Journal of the American Chemical Society*. Copyright 2017 American Chemical Society.

VII.A. Abstract

Protonated states of the nitrogenase active site are mechanistically significant since substrate reduction is invariably accompanied by proton uptake. We report the low pH characterization by X-ray crystallography and EPR spectroscopy of the nitrogenase molybdenum iron (MoFe) proteins from two phylogenetically distinct nitrogenases (*Azotobacter vinelandii*, Av, and *Clostridium pasteurianum*, Cp) at pHs between 4.5 to 8. X-ray data at pHs of 4.5 – 6 reveal the repositioning of sidechains along one side of the FeMo-cofactor, and the corresponding EPR data shows a new S = 3/2 spin state with spectral features similar to a state previously observed during catalytic turnover. The structural changes suggest that FeMo-cofactor belt sulfurs S3A or S5A are potential protonation sites. Notably, the observed structural and electronic low pH changes are correlated and reversible. The detailed structural rearrangements differ between the two proteins, which may reflect differences in potential protonation sites at the active site among nitrogenase species. These observations emphasize the benefits of investigating multiple nitrogenase species. Our experimental data suggests that reversible protonation of the resting state is likely occurring, and we term this state "E_0H^+", following the Lowe-Thorneley naming scheme.

VII.B. Introduction

Nitrogen fixation is the process of breaking the kinetically inert N-N triple bond via either reduction or oxidation of molecular dinitrogen. Biologically, nitrogen fixation is accomplished by the enzyme nitrogenase to yield ammonia, with an overall reaction stoichiometry conventionally described by Equation VII-1.

Equation VII-1. Biological nitrogen fixation

$$\mathrm{N_2 + 10H^+ + 8e^- + 16ATP \rightarrow 2NH_4^+ + H_2 + 16ADP + 16P_i}$$

Nitrogenase is a highly oxygen-sensitive enzyme present in specialized microorganisms; it consists of two proteins called the molybdenum-iron (MoFe) and iron (Fe) proteins.[26,33,128] The Fe protein contains two nucleotide binding sites and a 4Fe:4S cluster. The MoFe protein incorporates two 8Fe:7S "P-clusters" and two 7Fe:9S:C:Mo:*R*-homocitrate "FeMo-cofactors", the latter of which represents the active site where substrates bind and are reduced. ATP-dependent electron transfer occurs from the 4Fe:4S cluster to the P-cluster during docking interactions between the Fe and MoFe proteins, after which the proteins separate.[31,40,45] Substrates can only bind to forms of the FeMo-cofactor more reduced than the resting state. These states are conventionally designated as E_n, where *n* represents the number of electrons transferred to the MoFe protein (per active site); E_0 is the resting state.[40] Following the Lowe-Thorneley model, dinitrogen binds to the FeMo-cofactor in the E_3 and E_4 states; however, other substrates, such as acetylene, may bind to the FeMo-cofactor in less highly reduced states.[45]

Electron paramagnetic resonance (EPR) is a powerful tool for studying the electronic states of the FeMo-cofactor since the E_0 state exhibits a strong, unique rhombic spectrum, resulting from transitions within the ±1/2 ground-state Kramers' doublet of a $S = 3/2$ system.[129]

In contrast, the P-cluster is diamagnetic in the dithionite-reduced form (P^N) and exhibits a weak resonance at g = 12 in the oxidized form (P^{ox}).[130,131] The reported EPR spectra of the FeMo-cofactor under turnover conditions include three spin states called 1a, 1b, and 1c.[132–134] 1a is the resting state (E_0); 1b and 1c, which are in equilibrium with 1a,[134] are attributed to E_2 and are thought to represent different states of the FeMo-cofactor during turnover. More specifically, 1c is assigned to protonation of the FeMo-cofactor.[133] The E_1 state is EPR-silent.

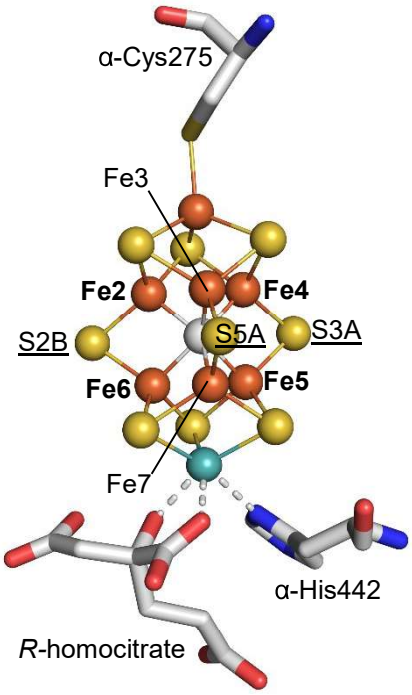

Figure 1. Structure of the FeMo-cofactor. The atoms of the cluster are shown in spheres and colored by element (Fe, orange; S, yellow; C, gray; Mo, cyan). Fe sites in the trigonal prism around the interstitial carbide are labeled. Belt S are also labeled and underlined. Coordinating residues and the R-homocitrate are shown in sticks and colored by element (C, gray; O, red; N, blue).

The FeMo-cofactor (Figure VII-1) contains a 7Fe:9S:C:Mo:homocitrate cluster exhibiting approximate C_{3v} symmetry. The core of the FeMo-cofactor is provided by a trigonal prism of six

Fe atoms (Fe2-7) surrounding an interstitial carbide.[22,72,135] Each face of the trigonal prism is bridged by one of three "belt" S labeled S2B, S3A, and S5A. Crystallographic evidence for turnover-dependent rearrangements of belt sulfurs is demonstrated by the reversible displacement of S2B upon CO inhibition.[37] Se from selenocyanate may also substitute S2B.[38] In the presence of substrate and under turnover conditions, interchange of the belt sulfurs was established such that Se originally at S2B migrates to S5A and S3A before ultimately exiting the FeMo-cofactor.[38] Intriguingly, the S2B site displaced by CO spans Fe2 and Fe6, which have been shown to be more oxidized in the resting state,[136] suggesting that their reduction is critical for ligand binding at this site.

There is still a high level of uncertainty in the mechanistic description of biological nitrogen fixation, including possible structural rearrangements in the FeMo-cofactor. The challenge has been to generate significant populations of higher E_n states competent for substrate binding. As formation of these states is associated with proton uptake, we reasoned that by studying the MoFe protein at low pH (high proton concentration), features of the active site that are characteristic of more highly reduced forms might be stabilized through Le Chatelier's principle. The effects of low pH (pH ≤ 5) on the X-ray structure and EPR spectra of the MoFe protein have not to our knowledge been described, likely because it has been reported that the MoFe protein is inactivated below pH 6.2.[137] However, our study shows that impacts to the atomic and electronic structure are reversible between pH 4.5 and pH 8.

In this study, we examine the two phylogenetically distinct nitrogenase MoFe proteins from *Azotobacter vinelandii* (Av1) and *Clostridium pasteurianum* (Cp1), which have a sequence identity of ~36%.[24] Working with Cp1 and Av1, we combine a structural approach with EPR spectroscopy to examine the atomic and electronic structure of MoFe proteins at pH 5 where the proton concentration is 2-3 orders of magnitude greater than that of typical enzyme activity

measurements. Changes occurring in the MoFe protein at low pH might therefore provide crucial information about the atomic and electronic structure of the protein at an early stage of substrate reduction.

VII.C. Results and Discussion

Over the pH range between 4.5-5.75, X-ray crystal structures of Cp1 and Av1 (Table VII-1) reveal structural rearrangements near the Fe3,4,5,7 face of the FeMo-cofactor (Figure VII-2) that are fully reversible upon returning to pH 8. For these studies, the purified protein was resuspended in a low pH tri-buffer system,[138] allowing the pH of the protein solution to be varied from pH 2 to pH 7 with minimal variation in the ionic strength and buffer components. Av1 and Cp1 exhibit a partially and fully occupied low pH conformer, respectively, when pH $\leq$ 5. We determined the pH 5 structures of Cp1 and Av1 at resolutions of 1.85 Å and 2.30 Å, PDB IDs 5VPW and 5VQ4, respectively. At pH ~6.5, Cp1 exhibits both conformations; the PDB ID for this structure is 5VQ3.

The conversion of the pH 8 to the low pH conformer under different pH and ionic strength was explored in Cp1 over a large number of conditions. It was found that higher ionic strength contributes to increased occupancy of the low pH conformer, which occurred at pH 5.8 or lower, depending on ionic strength. In view of the dependence of conformer occupancy on pH and ionic strength, as well as the challenges of measuring pH in small volumes around crystals and the uncertainties in extrapolating pH values measured to room temperature to the cryogenic temperatures used for crystallography and EPR, for simplicity, the acid-induced Av1 and Cp1 structural rearrangements are herein referred to as the low pH or pH 5 conformers.

At low pH in Cp1, a peptide flip[139] occurs between α-Ser346 and α-Arg347 (corresponding to Av1 residues, α-Leu358 and α-Arg359, respectively), causing the arginine

sidechain to reposition away from the face of the FeMo-cofactor (Figures VII-2b,3). Notably, this low pH rearrangement causes changes in hydrogen bonding interactions between sidechain atoms of α-Arg347 and S3A and S5A in Cp1 (Figure VII-3): (1) S5A loses its only hydrogen bond to NH1, (2) S3A loses its contact with the amide NH, and (3-4) S3A gains contacts with NH1 and NE. In Av1 at low pH, the sidechain of Av1 α-His274 (adjacent to the FeMo-cofactor ligand α-Cys275 and corresponding to Cp1 α-Gln261) moves closer to the FeMo-cofactor and displaces a water molecule. At this new position, a water molecule bridges the Av1 α-His274 sidechain and S5A of the FeMo-cofactor (Figure VII-2c). Of the two residues most affected by low pH in Cp1 and Av1, Cp1 α-Arg347 is invariant in all nitrogenases, whereas Av1 α-His274 is variant.[24] Mutagenesis of these residues in Av1 significantly reduces substrate reduction,[140,141] and α-His274 has been implicated in FeMo-cofactor insertion during Av1 assembly.[109]

Table VII-1. X-ray crystallographic data collection and refinement statistics

	Av1 at pH 5 (5VQ4)	Cp1 at pH 5 (5VPW)	Cp1 at pH 6.5 (5VQ3)
Data Collection Statistics			
Space group	$P2_1$	$P2_1$	$P2_1$
Cell dimensions a, b, c (Å); α, β, γ (°)	81.32, 128.9, 108.4 90, 110.9, 90	69.62, 146.3, 116.7 90, 103.6, 90	69.48, 148.0, 116.7 90, 103.5, 90
Resolution (Å)	39.54-2.30 (2.30-2.34)*	39.19-1.85 (1.88-1.85)*	39.83-1.75 (1.75-1.72)*
R_{merge}	0.174 (0.720)*	0.105 (0.684)*	0.079 (0.682)*
I/σ(I)	9.2 (3.1)*	11.6 (2.5)*	13.5 (2.9)*
Completeness (%)	98.8 (99.4)*	98.4 (95.4)*	98.4 (98.4)*
No. unique reflections	91,309 (4,321)*	189,858 (1,197)*	238,230 (11,876)*
Redundancy	6.7 (7.1)*	6.5 (6.2)*	6.8 (7.0)*
Refinement Statistics			
R_{work} / R_{free}	0.176 / 0.226	0.167 / 0.201	0.159 / 0.185
Average B-factor	24.0	30.0	29.0
R.m.s. bond lengths (Å)	0.011	0.012	0.013
R.m.s bond angles (°)	1.39	1.41	1.52

*Highest resolution shell is shown in parentheses.

The low pH structural rearrangements only occur on the face of the FeMo-cofactor that is exposed to water molecules (Fe3,4,5,7), potentially implicating this water pool (and likely the water channel that connects this pool to the protein surface) in proton transport between the active site and the exterior.[78,102,104] Additionally, there is slight movement (<1 Å) of the C1 carboxyl of the *R*-homocitrate *away* from α-Gln191 in Av1. A previously reported structure of Av1 at high pH shows slight movement of the C1 carboxyl *toward* α-Gln191,[142] which, in combination with results reported herein, indicates conformational flexibility in the C1 arm of the *R*-homocitrate in response to pH, possibly due to change in protonation state of the carboxylate group.

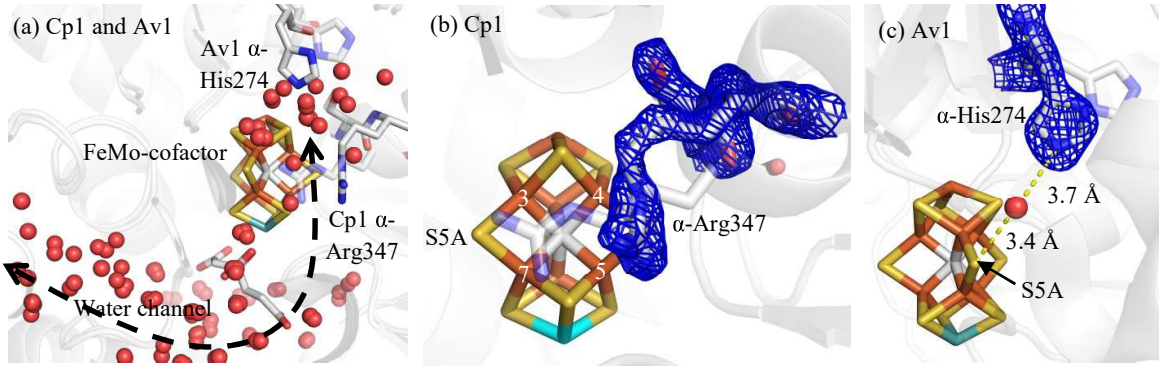

Figure VII-2. (a) Overview of the structural rearrangements observed at low pH at the active sites of Cp1 and Av1. Both changes occur on the Fe3,4,5,7 face of the FeMo-cofactor, which is the same face that is exposed to water molecules and connects to the interstitial water channel (dashed black line). (b) In Cp1, a peptide flip occurs between α-Arg347 and α-Ser346. Also, the Arg sidechain relinquishes its hydrogen bond with S5A and withdraws from the Fe3,4,5,7 face of the FeMo-cofactor. (c) In Av1, the α-His274 sidechain swings closer to the FeMo-cofactor and displaces a water molecule; two water molecules fill the former α-His274 sidechain position. The α-His274 coordinates to S5A of the FeMo-cofactor through a hydrogen bond bridge with a water molecule. In all images, transparent gray represents physiological pH structures. Non-transparent gray sticks show the low pH structural changes. The FeMo-cofactor and pH-affected residues are displayed as sticks and colored by element (yellow, S; orange, Fe;, cyan, Mo; gray, C). Water molecules are represented as red spheres. The blue meshes in (b) and (c) show the electron density maps of the pH affected residues contoured to 2.0 and 1.5 σ, respectively.

The low pH conformation changes could be triggered by proton binding to either the protein (possibly the sidechains of His, Glu, and Asp), as well as water and/or sites on the FeMo-cofactor such as the sulfurs and/or homocitrate. Without direct visualization of hydrogens, it is not possible to establish unambiguously which atoms are protonated to trigger the observed structural rearrangements. After close examination of the FeMo-cofactor and active site residues in the low pH and physiological pH structures, we see no obvious indicators for protonation of sidechains. It is also conceivable that protonation could be coupled to anion binding, such as buffer or counter-ion components in the buffer, but we see no evidence for this possibility, based on no appearance of new or shifted peaks in the solvent region. This leaves the possibility that the low pH rearrangements may reflect protonation of water and/or the FeMo-cofactor. Other than the homocitrate, the sulfurs represent the most likely site of protonation on the cofactor based on the pH titration properties of synthetic and protein-based clusters.[143–145]

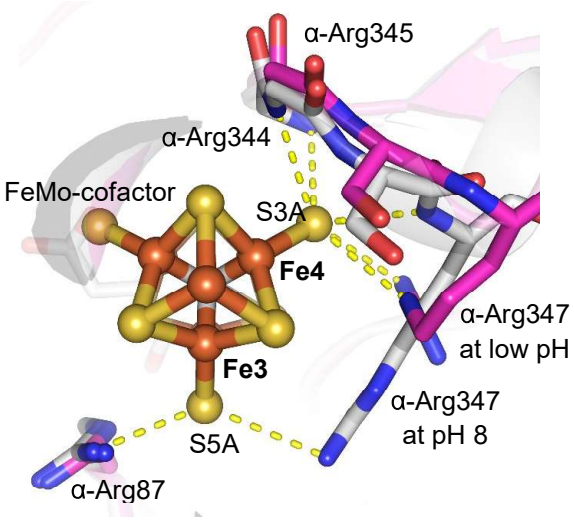

Figure VII-3. Structure of the Cp1 FeMo-cofactor as viewed down the C_3 axis. α-Arg347 at pH 8 (gray) and low pH (magenta) is shown in sticks. Contacts with the FeMo-cofactor at pH 8 and low pH are indicated with dashed yellow lines. All contact distances are ≤3.5 Å. The atoms of the cluster are shown in spheres and colored by element (Fe, orange; S, yellow; C, gray; Mo, cyan). Relevant Fe and S atoms are labeled. Coordinating residues and the *R*-homocitrate are shown in sticks and colored by element (C, gray; O, red; N, blue).

Following structural characterization by X-ray crystallography, EPR spectroscopy was performed on Cp1 and Av1 in solution at pH 8, 6.5, pH 5 (Figure VII-4). From simulations, the effective *g* values and *E/D* ratios were determined (Table VII-2 and Figure VII-S1). In both Cp1 and Av1, low pH conditions induce a second rhombic spin system with higher rhombicity compared to the resting state spin system at physiological pH. Line broadening is also observed in the low pH spectra, reminiscent of the EPR spectra of Cp1 FeMo-cofactor isolated in N-methylformamide. The two spin systems are in equilibrium with each other (Figure VII-4). All low pH EPR changes are reversible in both Cp1 and Av1 (Figure VII-S2). Power sweeps at low and physiological pH on Av1 and Cp1 show similar changes in peak area with change in power, indicating similar relaxation behavior of the resting state and low pH spin systems. Similar relaxation behavior is only expected for spin systems of the same cluster. Thus, the power sweeps demonstrate that both spin systems result from electronic changes at the FeMo-cofactor (Figure VII-S3).

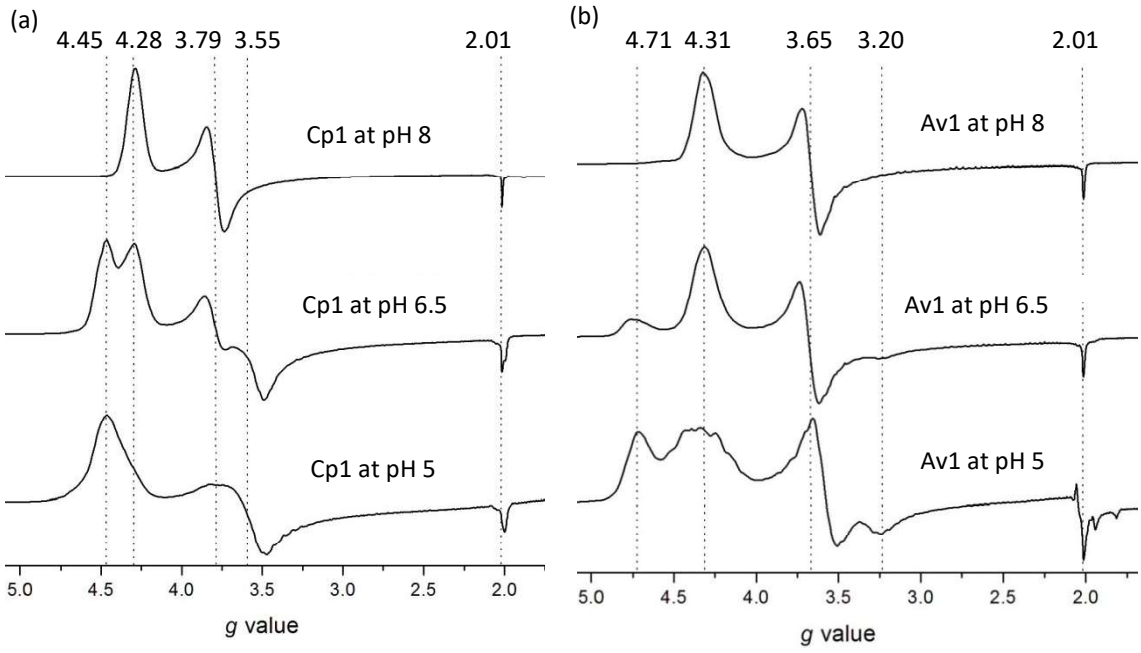

Figure VII-4. (a) Comparison of Cp1 at pH 8, pH 6.5, and pH 5. The same is shown in (b) for Av1.

The Av1 low pH spin state is an S = 3/2 system with zero-field splitting parameters similar to those reported for the 1c spin state. The 1c spin state emerges after 1b, putatively during the accumulation of electrons from the E0 to E2 state.[132] The 1c and 1b spin states form under turnover conditions (ATP regenerating system, Fe protein, and reductant) but without added substrate beyond H^+. 1c was never observed without 1b present,[132] and these signals relax with the same decay constant.[134] Follow-up studies on the EPR of states more reduced than E_0 suggest that 1c is a result of protonation of the FeMo-cofactor.[133]

Table VII-2. Summary of EPR data

Protein		g_{eff} values*	*E/D*	References
Resting state Cp1 at pH 8		4.28, 3.79, 2.01	0.041	This work
		4.29, 3.76, 2.01	Not reported	[146]
Cp1 at pH 6.5		4.28, 3.79, 2.01 (physiological pH spin state)	0.041	This work
		4.45, 3.55, 2.00 (low pH spin state)	0.077	
Cp1 at pH 5		4.45, 3.60, 2.00	0.070	This work
Av1 resting state at pH 8		4.30, 3.65, 2.01	0.053	This work
		4.31, 3.65, 2.01	0.053	[147]
Av1 under turnover conditions at pH 8	1a	4.32, 3.66, 2.01	Not reported	[34,132,134]
	1b	4.21, 3.76, 1.97	Not reported	[34,133,134]
	1b	4.27, 3.73, 2.02	Not reported	[132]
	1c	4.7 or 4.69, ~3.2-3.4, ~2.0	Not reported	[132–134,148]
Av1 at pH 6.5		4.31, 3.67, 2.01 (physiological pH spin state)	0.053	This work
		4.72, 3.30, 2.01 (low pH spin state)	0.124	
Av1 at pH 5		4.32, 3.57, 2.01 (physiological pH spin state)	0.064	This work
		4.71, 3.30, 2.01 (low pH spin state)	0.120	

* Effective *g* values are reported for simulated EPR spectra.

The equivalence between the crystal structure and the protein in solution was accomplished by measuring the EPR spectrum of a solution and polycrystalline protein sample under the same conditions used for the low pH X-ray crystallographic experiments (Figure VII-

S4). The resulting spectra exhibit the same features, thereby confirming that the low pH structural changes observed by X-ray crystallography correlate to the low pH electronic changes observed by EPR spectroscopy.

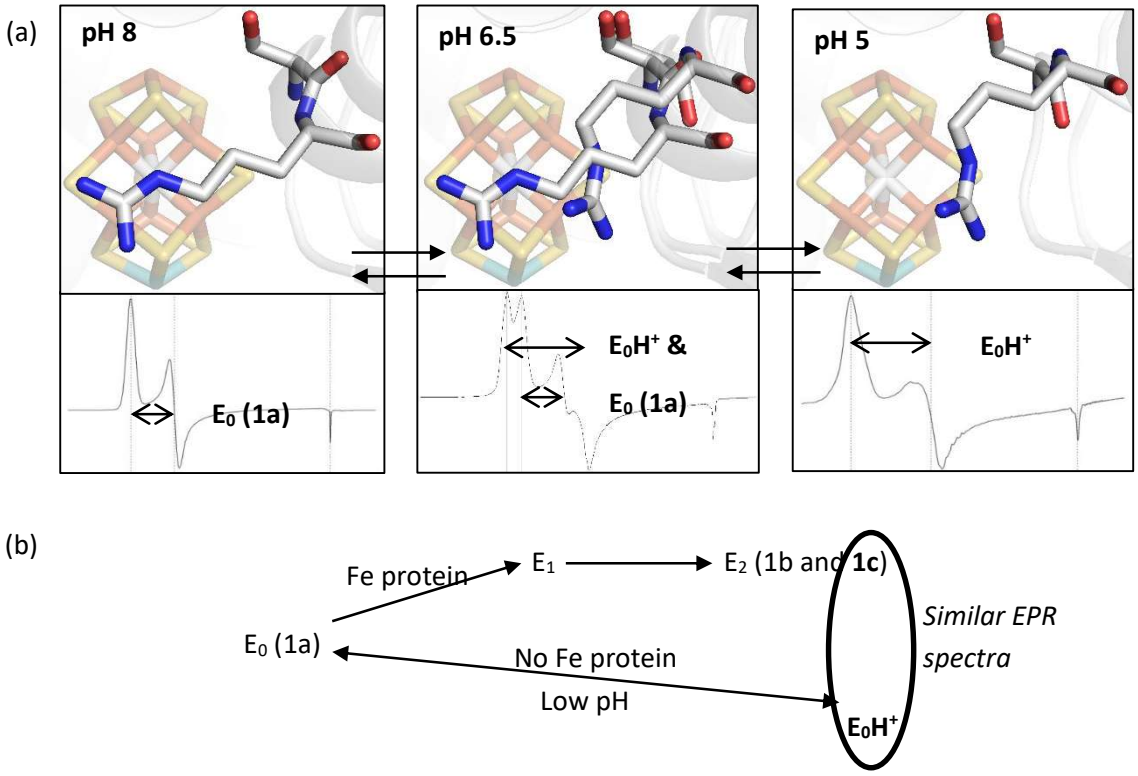

Figure 5. (a) A summary of the Cp1 data presented in this manuscript. At pH 8, the typical resting state X-ray diffraction structure and EPR signal are observed. At pH 5, a peptide flip and repositioning of the α-Arg357 sidechain away from the Fe3,4,5,7 face of the FeMo-cofactor is observed as well as an EPR signal similar to that reported for the E_2 state. At intermediate pH, both structural conformations and EPR states are observed. The EPR signals and X-ray structures are reversible and correlated. (b) The 1c peak has been attributed to the E_2 state and is hypothesized to result from protonation of the FeMo-cofactor. Our experimental conditions include only a proton source and not an electron source, so it is unlikely that these conditions achieve a reduced state, such as E_2. Given the similarity to the 1c peak and our experimental conditions, it is more likely that the resting state is protonated, which we have termed "E_0H^+".

Because our experimental conditions do not include the Fe protein and ATP regenerating system, and because all data obtained with and without dithionite are comparable, a net flow of

electrons to the FeMo-cofactor is likely not occurring in our low pH experimental conditions. Therefore, we conclude that the low pH state is a protonated resting state. We call it "E_0H^+", following the Lowe-Thorneley naming scheme. We would like to emphasize that this name is a generic designation for a protonated form of the resting state; we cannot determine the number of protons added to the FeMo-cofactor at low pH. Figure VII-5 depicts a summary of the relationships between different forms of the resting state, together with their major X-ray and EPR features.

VII.D. Conclusion

The active site of the MoFe protein exhibits pH-dependent structural and electronic rearrangements localized at the active site. The low pH structural rearrangements involve residues α-Arg347 from Cp1 and α-His274 from Av1, both of which participate in hydrogen bond networks with FeMo-cofactor belt sulfurs. The structural and electronic changes are reversible with pH and directly correlated, the latter of which was demonstrated by performing EPR spectroscopy on polycrystalline samples. The low pH Av1 spin system has EPR spectral features similar to that observed for 1c, which is one of the two spin states assigned to E_2. Given the observed structural rearrangements and the absence of net flow of electrons through nitrogenase at low pH without the Fe-protein, we conclude that reversible protonation of the resting state of the FeMo-cofactor occurs at low pH to generate "E_0H^+."

This study demonstrates the advantage of comparing more than one species of nitrogenase MoFe protein, despite having the same cofactor structures, when addressing the mechanism of substrate reduction. This is supported by the fact that the low pH structural and electronic changes of Cp1 and Av1 are similar but not identical: the low pH structural changes occur on the same face of the FeMo-factor but not the same residue, and the low pH spin states

show similar but not identical *g* values and *E/D* ratios. In both Cp1 and Av1, however, the structural data suggest protonation of the resting state may occur at one of the two belt sulfurs that are not replaced by CO or Se, which may facilitate rearrangements of the cofactor during turnover.

VII.E. Experimental

VII.E.i. Cell growth and protein purification

Av1 and Cp1 protein were obtained using cell growth and protein purification procedures previously described.[64,73]

VII.E.ii. Crystallization

Protein crystals were grown in 24-well plates using the sitting-drop method with a 1:1 ratio of protein stock to reservoir solution, at room temperature, and in an anaerobic chamber with an atmosphere of ~95% argon and ~5% hydrogen. All solutions were made anaerobic through a series of vacuum and argon cycles. The reservoir solution for Av1 crystals consisted of double-distilled water, 15% polyethylene glycol (MW 4000 g/mol, Hampton Research), 0.5-0.8 M sodium chloride (VWR), 0.2 M imidazole/malate at pH 8 (Sigma-Aldrich), and 5 mM sodium dithionite (J.T. Baker). The reservoir solution for Cp1 crystals consisted of double-distilled water, 13.5-14% polyethylene glycol (MW 3350 g/mol, Hampton Research), 0.3-0.5 M magnesium chloride (Mallinckrodt), 0.08 M Tris at pH 8 (Fisher Scientific), and 5 mM sodium dithionite. Av1 and Cp1 crystals of block morphology formed overnight.

VII.E.iii. Tri-buffer preparation

A tri-buffer consists of three different buffers, such that the buffering capacity extends over a large pH range while maintaining a nearly constant ionic strength. We created a tri-buffer from 0.05 M glycylglycine (pK_a = 3.14, Acros Organics), 0.05 M acetic acid (pK_a = 4.76, Sigma-Aldrich), 0.10 M Bis-Tris (pK_a = 6.46, Sigma) based off work on by Ellis and Morrison. The tri-buffer was adjusted to pH 6, 5, 4, 3, and 2 using HCl and maintained an ionic strength of ~0.1 M.

VII.E.iv. pH measurements

The pH of solutions surrounding crystals was measured using litmus paper at room temperature. Since the experimental conditions were 100 K (X-ray crystallography) and 4-8 K (EPR), the pH of the samples under cryogenic conditions will likely be greater than measured at room temperature.[149]

VII.E.v. X-ray sample preparation

A low pH solution was made according to the recipe for each well's reservoir solution except that a tri-buffer at low pH was substituted for Tris/HCl at pH 8. 10 µL of low pH solution was added to each well containing crystals as well as 1 µL of 2-methyl-2,4-pentanediol (cryo-protectant, Acros Organics). Also, three drops of Fomblin Y 16/6 mineral oil (Sigma-Aldrich) were added to the top of each crystal drop for additional cryo-protection. Crystals soaked for at least five minutes in the low pH solution before flash freezing in liquid nitrogen on nylon loops. The percentage of protein molecules exhibiting the low pH structural rearrangements was not impacted by soaking duration, provided that the crystals soaked for at least five minutes before freezing. Because the crystal wells contain Tris at pH 8 as part of the crystallization recipe, the actual pH that the crystals soaked in upon addition of low pH buffer was higher than the pH of

the added tri-buffers. To illustrate, in order to soak a crystal at pH 5, tri-buffer at pH 2 must be added to the crystallization well, since Tris at pH 8 is also present. Attempts to transfer crystals from the crystal well to a low pH buffer resulted in crystal cracking.

To check for reversibility in the crystallized state, crystals were soaked at low pH as described for 10 minutes, transferred to a well containing fresh reservoir solution at pH 8, and then flash frozen in liquid nitrogen after soaking for 5 minutes.

VII.E.vi. X-ray data collection and refinement

Diffraction data for Cp1 was collected remotely from the Stanford Synchrotron Radiation Light source (SSRL) on beamline 12-2 with a DECTRIS Pilatus 6 M detector. Reference sets of 1440 diffraction images were collected at 12999.97 eV with an oscillation angle of 0.25° over 360° rotation. Diffraction data for Av1 was collected in-house on a Rigaku MicroMax 007-HF X-ray generator with a Rigaku RAXIS-IV++ detector. All data sets were integrated with the XDS program package.[57] Scaling was carried out with the CCP4 suite,[58] and phasing was determined by molecular replacement against high resolution Av1 (PDB ID 3U7Q) and Cp1 (PDB ID 4WES) structures.[22,64] Initial refinement was carried out with CNS,[59] and alternative conformations and isotropic B-factors were refined with REFMAC5.[60,61] All figures were made in PyMOL.[63]

VII.E.vii. EPR sample preparation

After solubility tests, the following solution was chosen for low pH EPR studies: 100 mM tri-buffer at pH 2, 500 mM $MgCl_2$, and 5 mM sodium dithionite. To prepare the EPR samples, protein stock was concentrated 50% and then diluted with the low pH EPR solution. Samples were allowed to equilibrate for at least 30 minutes prior to freezing in liquid nitrogen. 200 µl of each sample (~30 mg/mL) was transferred to an EPR tube in an anaerobic tent. The samples

were carefully frozen in liquid nitrogen inside the anaerobic tent and then stored in a liquid nitrogen dewar until use.

After obtaining an EPR spectrum of the low pH Av1 and Cp1 samples, the samples were thawed and transferred to physiological pH by repeatedly concentrating the protein solution and then diluting it with the protein storage solution (200 mM NaCl, 50 mM Tris at pH 8, and 5 mM sodium dithionite). EPR spectroscopy was performed on the protein resuspended at physiological pH to check for reversibility.

To test if the structural changes observed by X-ray crystallography are related to changes observed in the solution state by EPR, polycrystalline samples of Av1 and Cp1 were made by collecting crystals from six plates of seeded crystals, crushing the crystals, and transferring them to low pH solutions used for the X-ray studies: (Av1) 15% PEG 4000 g/mol, 0.5 M $MgCl_2$, 0.1 M tri-buffer at pH 2, 5 mM sodium dithionite; (Cp1 partial peptide flip) 14% PEG 3350 g/mol, 0.3 M $MgCl_2$, 0.02 M tri-buffer at pH 2, 5 mM sodium dithionite; (Cp1 complete peptide flip) 13.5% PEG 3350 g/mol, 0.5 M $MgCl_2$, 0.08 M tri-buffer at pH 2, 5 mM sodium dithionite.

VII.E.viii. EPR spectroscopy

EPR spectra were recorded with an X-band Bruker EMX spectrometer equipped with an ER 4119HS cavity. The Bruker Win-EPR software suite version 3.0 was used. Variable temperature experiments were performed with an Oxford (ESR900) helium cryostat (temperature range 4-8 K). All spectra were recorded at 9.37 GHz with a microwave power of 1 mW, a modulation amplitude of 2 G, and a modulation frequency of 100 kHz at 4 K. For the power sweep data, the power was varied from 0.02 mW to 20 mW and the temperature was set to 5 K and 8 K for Av1 and Cp1, respectively. Simulations were performed with the EasySpin software suite (Figure VII-S6).[150] For all simulations, the S = 3/2 real spin system (axial *g*-tensor) and S = 1/2 effective spin

system (rhombic *g*-tensor) were matched to the experimental spectra. From the S = 3/2 model, the *E/D* ratio was determined; from the S = 1/2 model, the effective *g* values were determined. For spectra exhibiting two spin states, simulations were calculated by combining two spin systems with their own *E/D* ratios and *g* values. The relative weight of the spin systems and line widths were varied by inspection. All parameters for the simulations are provided in Table VII-S2.

VII.F. Acknowledgement

We acknowledge the Gordon and Betty Moore Foundation and the Beckman Institute at Caltech for their generous support of the Molecular Observatory at Caltech. We thank the staff at Beamline 12-2, Stanford Synchrotron Radiation Lightsource (SSRL), operated for the DOE and supported by its OBER and by the NIH, NIGMS (P41GM103393), and the NCRR (P41RR001209). We thank Dr. Angelo Di Bilio for assisting with the EPR experiments; Dr. Lorenz Heidinger for providing a script for EPR simulations; Dr. Paul Oyala for assistance with the EPR simulations and analysis; Dr. Jens Kaiser, Dr. Kathryn Perez, Dr. Helen Segal, Belinda Wenke, and Renee Arias for helpful discussions.

VII.G. Supporting Information

Figure VII-S1. EPR simulations (see Table VII-S1 for simulation parameters)

(a) Cp1 EPR simulations at pH 8, 6.5, and 5

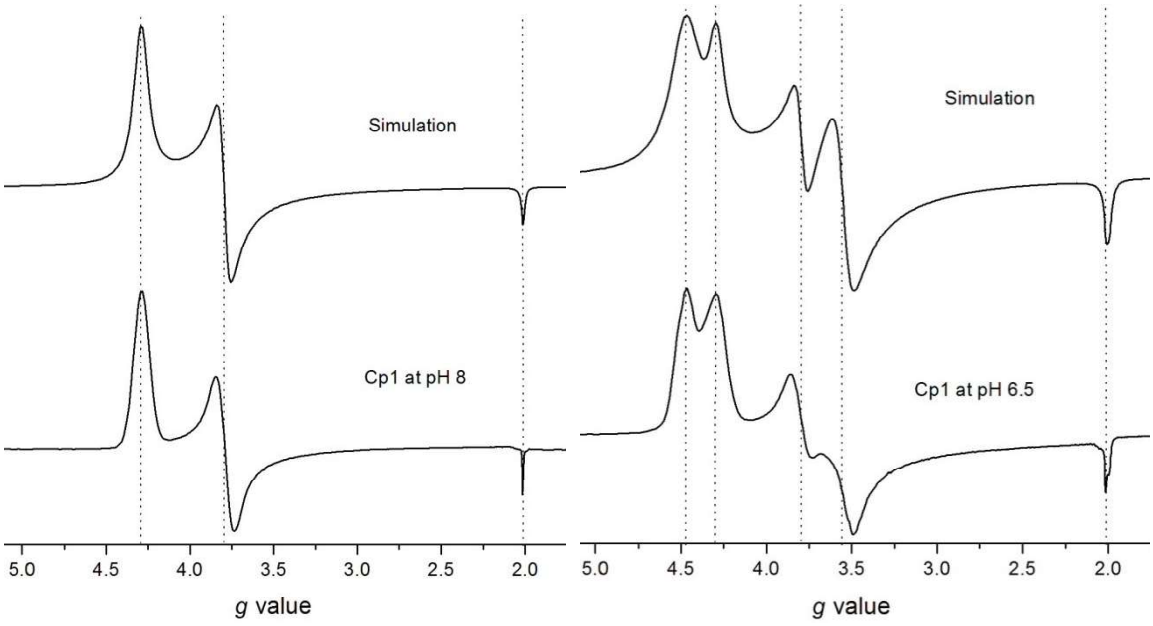

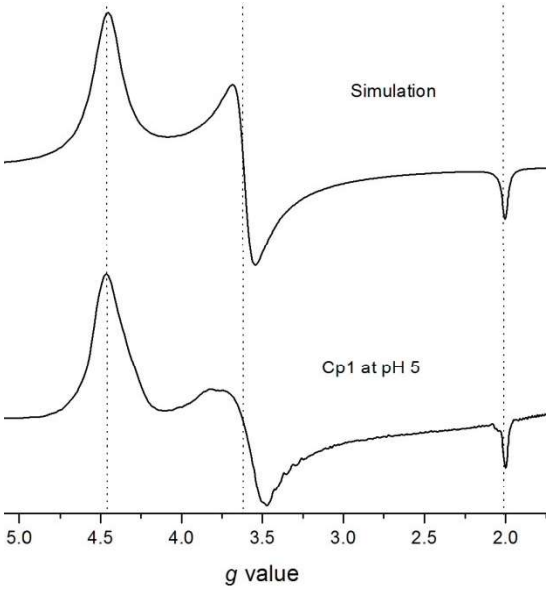

(b) Av1 EPR simulations at pH 8, 6.5, and 5

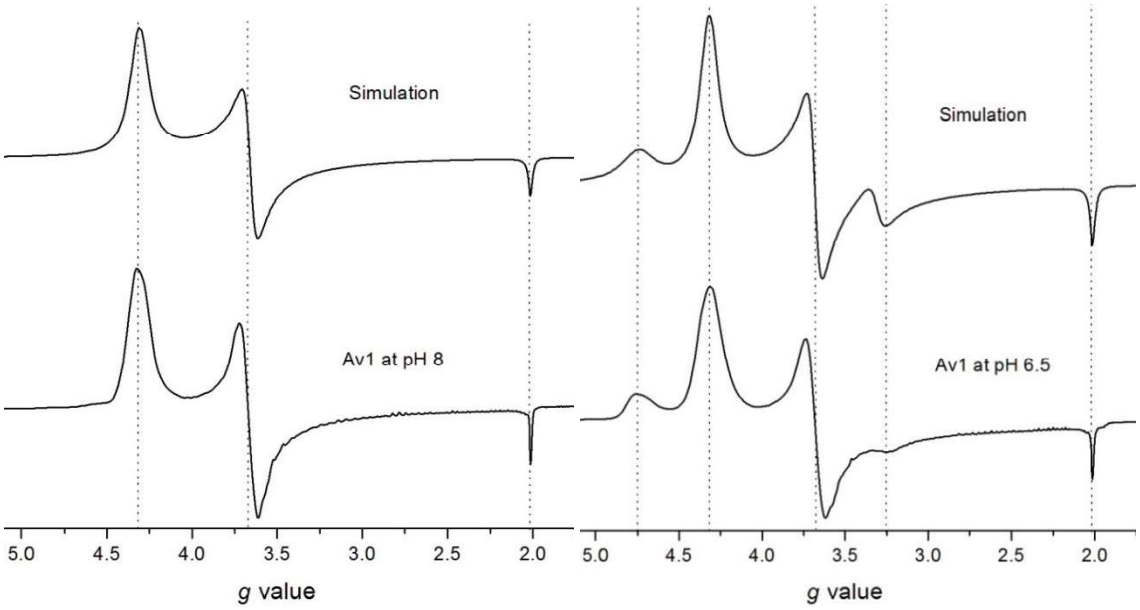

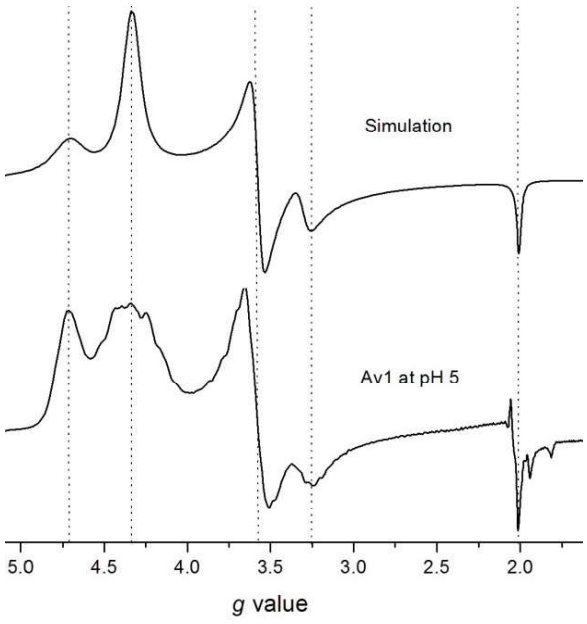

Table VII-S1. Parameters of EPR simulations

	Cp1				**Av1**				
	pH 8	pH 6.5		pH 5	pH 8	pH 6.5		pH 5	
		A	B			A	B	A	B
***S* = 3/2 model**									
E/D	0.041	0.041	0.077	0.07	0.0545	0.053	0.12	0.064	0.12
line width	1, 2	1, 2	1, 4	1, 4	1, 2.5	1, 2.5	1, 4	1, 2.5	1, 4
***S* = 1/2 model**									
g values	4.28 3.79 2.01	4.28 3.79 2.01	4.45 3.55 2.00	4.45 3.60 2.00	4.30 3.65 2.01	4.31 3.67 2.01	4.72 3.30 2.01	4.32 3.57 2.01	4.71 3.30 2.01
weight	n/a	1	4	n/a	n/a	3	1.5	3	1.5

For all simulations, the *S* = 3/2 real spin system (axial *g*-tensor) and *S* = 1/2 effective spin system (rhombic *g*-tensor) were matched to the experimental spectra. To determine the *E/D* ratio from the *S* = 3/2 model, the *E/D* ratio was varied while the *g* values were kept within 1% of [2.00 2.00 2.02]. From the S = 1/2 model, the effective *g* values were determined. For spectra exhibiting two spin states, simulations were calculated by combining two spin systems with their own *E/D* ratios and *g* values. The relative weight of the spin systems and line widths were varied by inspection. (Copied from Experimental Section in the main text.)

Figure VII-S2. The electronic changes at the FeMo-cofactor observed by EPR at low pH are reversible in Cp1 and Av1

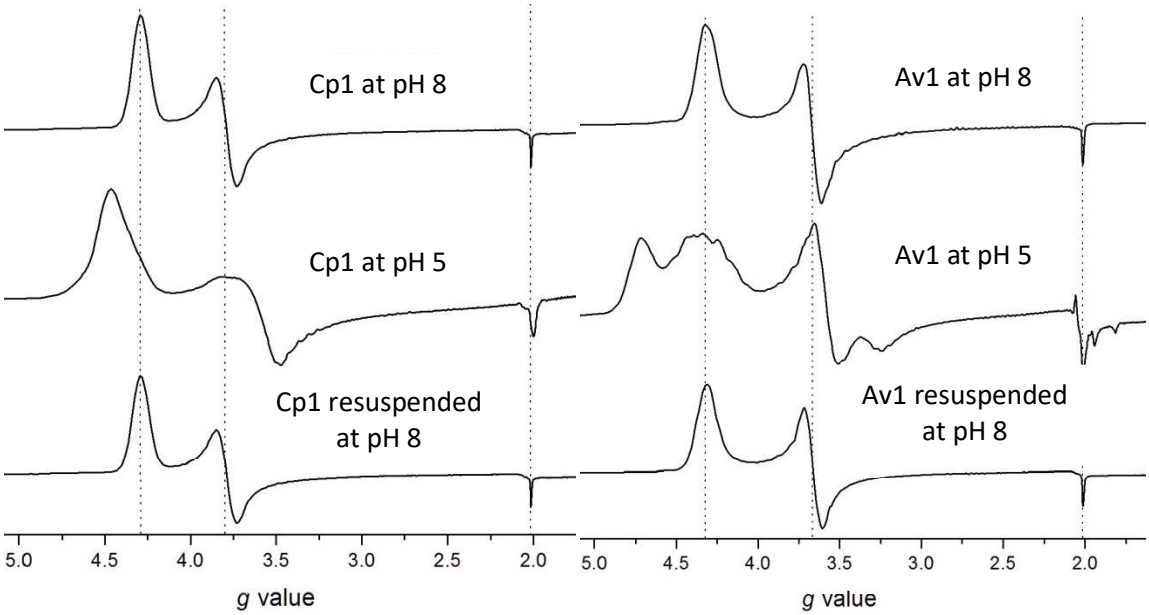

Low pH Av1 and Cp1 samples were resuspended at pH 8. This EPR of the reconstituted protein matches the EPR spectra of native protein, indicating that the electronic changes at the FeMo-cofactor are reversible with pH.

Figure VII-S3. Power Sweep of Cp1 and Av1 at physiological and low pH

(a) Cp1 Power Sweep at pH 8

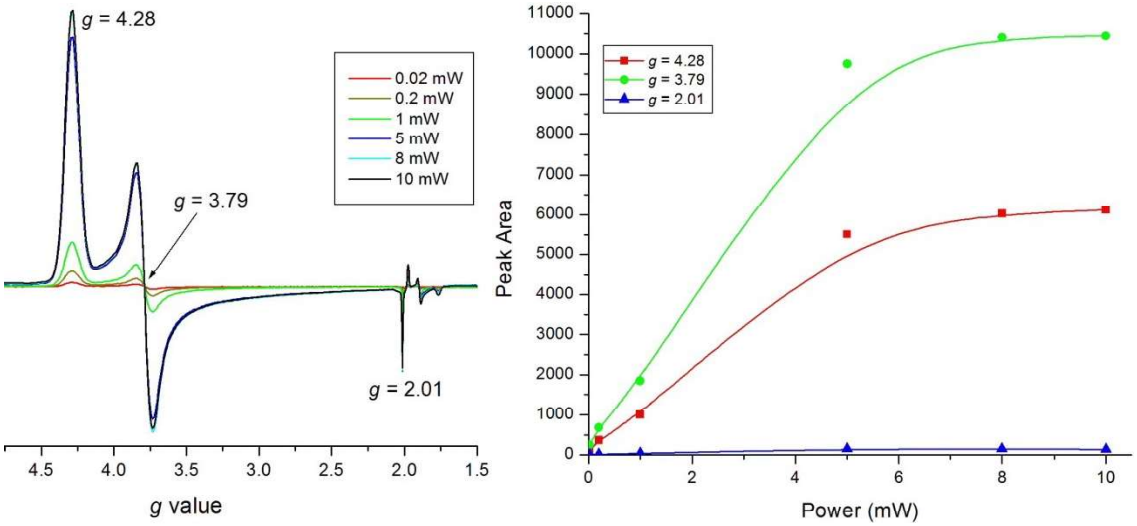

(b) Av1 Power Sweep at pH 8

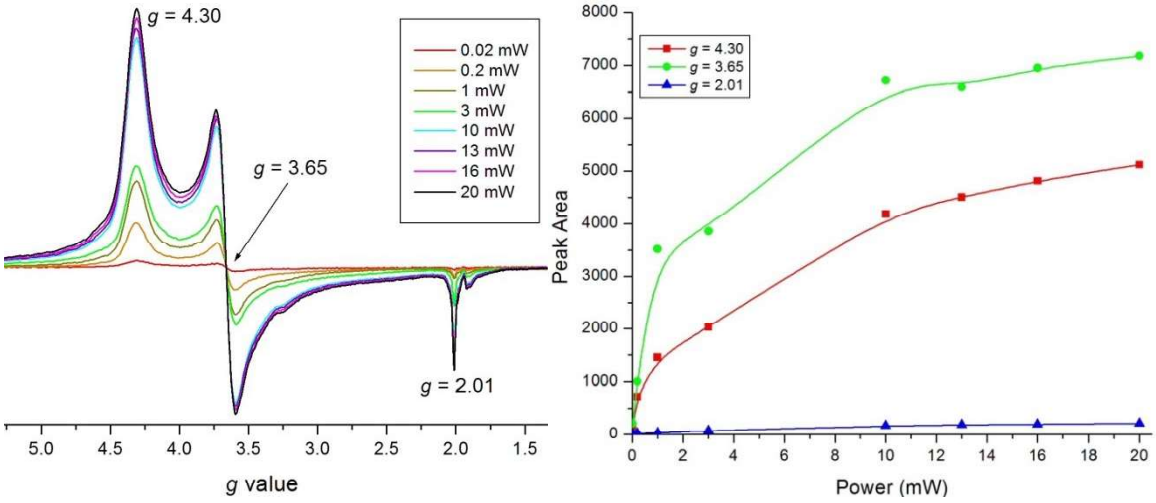

(c) Cp1 Power Sweep at pH 6.5

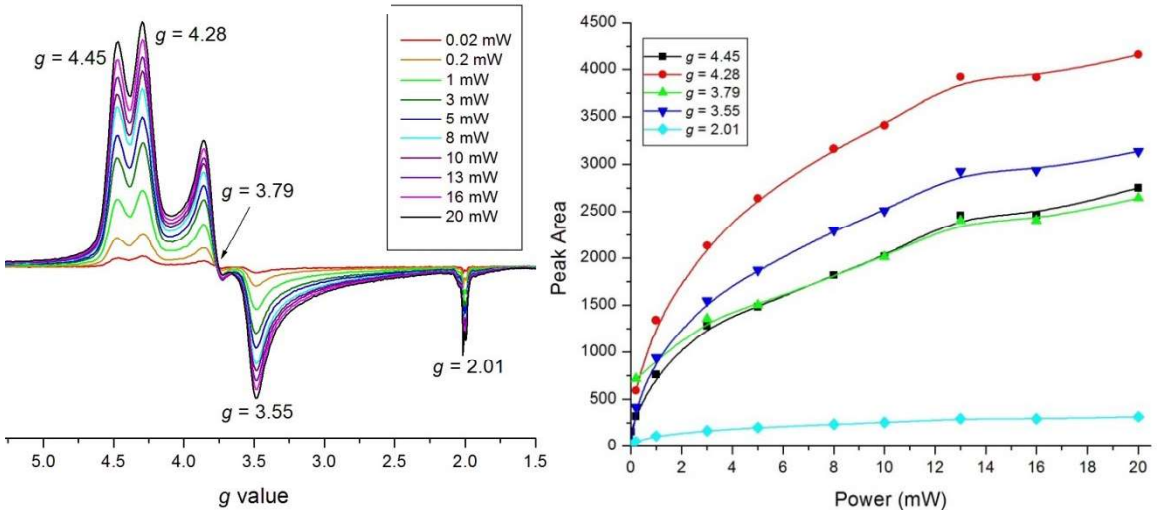

(d) Av1 Power Sweep at pH 6.5

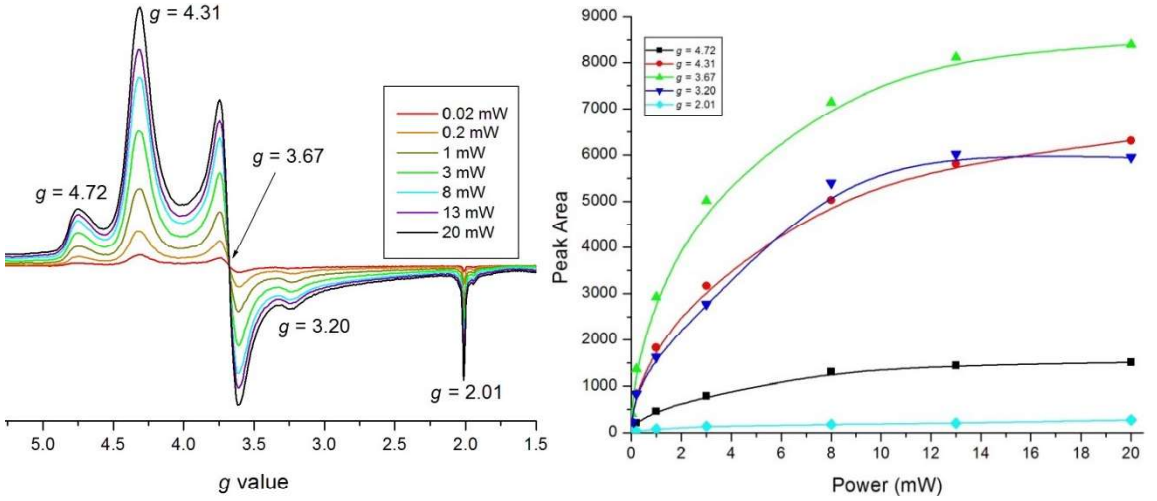

All of the peak area curves show the similar relaxation behavior, indicating that all observed peaks are a result of unpaired spins in the FeMo-cofactor and its environment.

Figure VII-S4. Comparison of polycrystalline and solution protein for Av1 and Cp1 at low pH

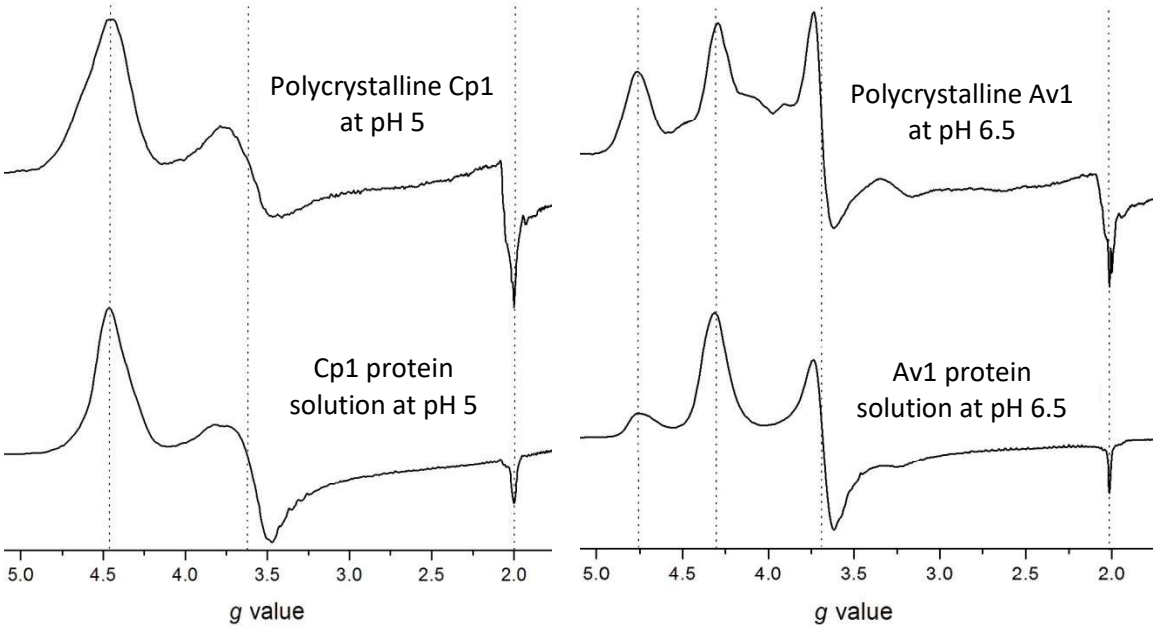

The EPR spectra of polycrystalline and solution protein at low pH match well for both Av1 and Cp1, indicating that the low pH structural changes observed by X-ray diffraction are the cause of changes observed in the EPR spectra at low pH.